Hip-Knee Motion-Lagged Coordination Mapping Enables Speed Adaptive Walking for Powered Knee Prosthesis

Yang Lv, Wen Zhang, Xiaoxu Zhang, *Member, IEEE*, and Jian Xu

***Abstract*— The commonly used finite-state-machine (FSM) impedance control for powered prostheses deploys diverse control parameters according to different gait phases, resulting in dozens of parameter adjustments and possible gait phase misrecognition. In contrast, this study presents a straightforward, continuous, and speed-adaptive control approach based on hip-knee motion-lagged coordination mapping (MLCM). The mapping, featured by the motion lag, can effectively generate the prosthetic knee's goal gait within a second-order polynomial. It is also verified from extensive gait analysis that the motion lag and polynomial coefficients evolve linearly with respect to walking speed and gait period, promising a simple real-time deployment for prosthesis control. Experimental validation with two non-disabled subjects and two transfemoral amputees wearing a prosthesis demonstrates the MLCM controller's ability to reduce the hip compensatory behavior, generate biomimetic knee kinematics, stance phase time, stride length, and hip-knee motion coordination across various speeds. Furthermore, compared to the benchmark FSM impedance controller, the MLCM controller reduces the number of control parameters from 17 to 7 and avoids misrecognition during gait phase transitions.**

***Index Terms*— Joint coordination, motion lag, gait planning, biomimetic gait, lower-limb prosthesis.**

I. Introduction

TO RESTORE the ability to walk, most lower-limb amputees use passive prosthetic legs, which will cause the compensatory behavior of healthy limbs [1] and cost more energy than healthy people. For example, when an amputee wants to swing the prosthesis, he/she should intentionally swing his/her residual hip joint to propel the prosthetic knee, increasing muscle energy metabolism. This can also lead to joint discomfort and back pain during daily usage [2]. A powered knee prosthesis can solve these problems by driving prosthetic joints with motors instead [3]. Hence, the question of how to drive the prosthetic joints emerges.

The most common approach is impedance control based on finite state machine (FSM) [4], [5]. This method divides the entire gait cycle into 4 to 5 phases according to joint angle, angular velocity, or ground reaction force criteria and adjusts impedance parameters for each phase. Although this method is relatively simple to deploy, it usually involves 20 to 30 control parameters, resulting in several hours of parameter tuning [6]. Furthermore, different finite-state machines must be designed for various gait modes, such as variable-speed or variable-slope motion. To reduce the time spent on parameter tuning, researchers use reinforcement learning method [7] and biologically-inspired parameter selection method (e.g., determining ankle impedance stiffness as a function of the user's body mass and ankle angle [8] or joint torques as functions of joint angle and walking speed [9]) to determine parameters automatically. While these methods reduce parameter tuning efforts for specific gait phases or modes, the control parameters still need to be switched between different gait phases and modes. Once the gait phase is misidentified, the prosthesis will move improperly, leading to sudden torque changes or sometimes a fall for amputees [10]. Therefore, researchers tried to seek a unified and continuous control method.

One way to develop a unified and continuous control method is to construct a phase variable [11] monotonically increasing with state variables. This phase variable can replace time over the gait cycle, allowing us to define desired joint trajectories in an autonomous mode. This way, continuous position control over the gait cycle can be achieved without dividing phases. Because of its continuity, the control parameters are significantly reduced. The most recognized phase variable, the polar coordinate of the hip's phase portrait [12], facilitated amputees walking at different speeds and inclines with a powered knee-ankle prosthesis, requiring only six control parameter adjustments [13]. Subsequent research extended the phase-based control to up and down stairs [14], volitional movements like kicking the ball, and backward walking [15]. However, the continuous phase variable is assumed to increase

Manuscript received 9 March 2024; revised 27 May 2024 and 14 July 2024; accepted 27 July 2024. Date of publication 30 July 2024; date of current version 5 August 2024. This work was supported in part by the National Natural Science Foundation of China under Grant 12372065, Grant 12372022, and Grant 11932015; and in part by Shanghai Municipal Science and Technology Major Project 2021SHZDZX0103. *(Corresponding author: Xiaoxu Zhang.)*

This work involved human subjects or animals in its research. Approval of all ethical and experimental procedures and protocols was granted by the Ethics Committee of Fudan University under Application No. FE23262I.

Yang Lv, Wen Zhang, and Jian Xu are with the Academy for Engineering & Technology, Fudan University, Shanghai 200433, China (e-mail: lvy21@m.fudan.edu.cn; 20110860045@fudan.edu.cn; jian_xu@fudan.edu.cn).

Xiaoxu Zhang is with the Academy for Engineering & Technology, MOE Frontiers Center for Brain Science, Fudan University, Shanghai 200433, China, and also with Yiwu Research Institute, Fudan University, Yiwu 322000, China (e-mail: zhangxiaoxu@fudan.edu.cn).

This article has supplementary downloadable material available at https://doi.org/10.1109/TNSRE.2024.3435931, provided by the authors.

Digital Object Identifier 10.1109/TNSRE.2024.3435931

monotonically at a constant rate. Sections of low thigh angular velocity break this rule because they cause a pause in the phase variable trajectory. Although the phase variable can be forced to increase uniformly during these sections by segmentation, this undoubtedly increases the complexity of constructing a phase variable [16]. If a direct mapping relationship between the hip and knee joints can be directly established, the prosthetic control would be more straightforward because constructing the phase variable can be omitted.

Our previous study [17] established a practical polynomial mapping from the lagged hip angle to the knee angle, namely MLCM (motion-lagged coordination mapping). In simulations, we verified that MLCM enables continuous speed-adaptive amputee walking with only two control parameters to adjust. However, firm modifications are still required to promote MLCM from numerical studies to real deployment. The first is to design a reasonable sensor layout and communication on the hardware platform to adapt the mapping flow. The second is to provide a new model coefficient training mode because the peak-based normalization [17] is no longer applicable in real-time data processing. The last step is to realize a reliable online estimation and deployment of motion lag, especially in the scenario of speed-changing walking.

To address the above issues, this paper (1) realized an IMU-encoder-load sensor embedded architecture to facilitate motion sensing and gait phase cognition for the MLCM controller, (2) modified MLCM by further associating model coefficients with walking speed to avoid real-time data normalization, and (3) selected a paradigm, including real-time walking speed estimation and data array shifting, for online estimation and deployment of motion lag. By solving these three issues, the article's most prominent contribution lies in experimentally validating a speed-adaptive controller for prosthetic knee joints based on hip-knee coordination mapping [17]. The MLCM controller is verified to reduce the hip compensatory behavior and generate biomimetic knee kinematics, stance phase time, stride length, and hip-knee motion coordination across various speeds. It also greatly reduces the number of control parameters and avoids misrecognition during gait phase transitions compared to the benchmark FSM impedance controller.

The article is organized as follows. In Section. II, we begin by introducing a newly built powered knee-ankle prosthesis. Next, we present the control method in detail, comprising a modified MLCM generator and a torque controller (Section. III). The MLCM generator includes real-time walking speed estimation and motion lag realization, which we validate in a preliminary experiment. Then, we perform validation experiments with two non-disabled subjects and two transfemoral amputees wearing a prosthesis, demonstrating the controller's excellence in various speed tasks (Section. IV). Furthermore, comparison with a benchmark FSM controller reinforces the advantages of our control methodology.

II. Hardware Setup

This section describes the actuation design and embedded system of the robotic knee-ankle prosthesis used for MLCM validation.

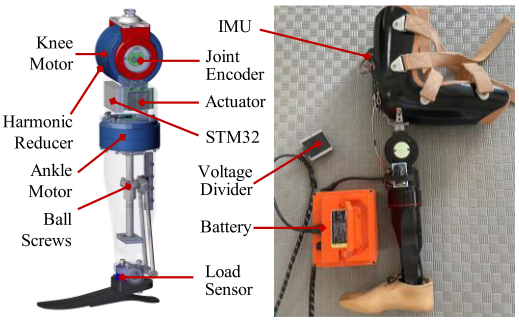

Fig. 1. Solidworks drawing and prototype of the powered prosthesis.

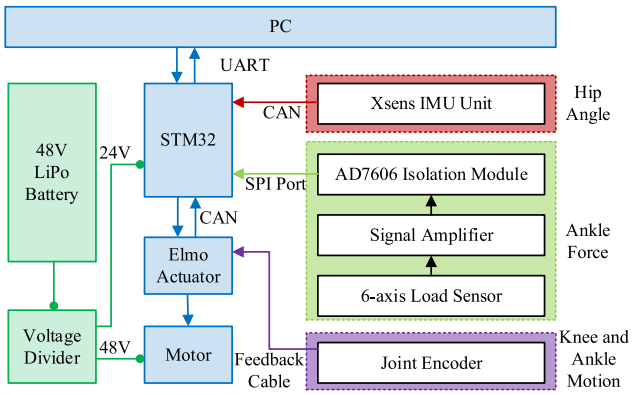

Fig. 2. Embedded system of the prosthesis.

A. Actuation Design

A powered knee-ankle prosthesis (shown in Fig. 1) is designed and fabricated at Fudan University as a research platform for testing the control strategies. It is tailored to match the kinematics and dynamics required for a 170 cm, 75 kg non-disabled person [17]. The knee and ankle joints are powered by high-torque motors (RI80 KV75, T-motor, China). The knee joint has a range of motion from -5° to 120° with a sustained torque of ∼110 N·m, while the ankle joint offers a range from -35° to 35° with a sustained torque of ∼90 N·m. The rated torque is comparable to state-of-the-art prosthetic limbs [18]. The knee joint is actuated by a harmonic drive (CAD-20-50-2A-GR, Harmonic Drive, Japan) with a transmission ratio of 50, while the ankle joint employs a 10 mm diameter and 5-mm ball screw linkage transmission. The prosthesis weighs about 4.5kg, with most components constructed from 7075-T6 aluminum alloy and a few shafts and bearings made of #45 steel.

B. Embedded System

As depicted in Fig. 2, the embedded system consists of a power supply system, a control unit, and a sensing system. A 48 V/20 Ah LiPo battery powers the control board and the motor through a tether. To prevent voltage overshoot, a voltage divider divides 24 V to the control board and 48 V to the motor. The control unit integrates an STM32F407 microprocessor (STM32F4, ST, Switzerland), two actuators (G–MOLTWIA50/100EEOT, Elmo, Israel), and two high-torque motors. The microprocessor calculates and sends the current command to the actuators via CAN, which controls the motors in a three-phase manner. During real-time control, the microprocessor can wirelessly transmit data to

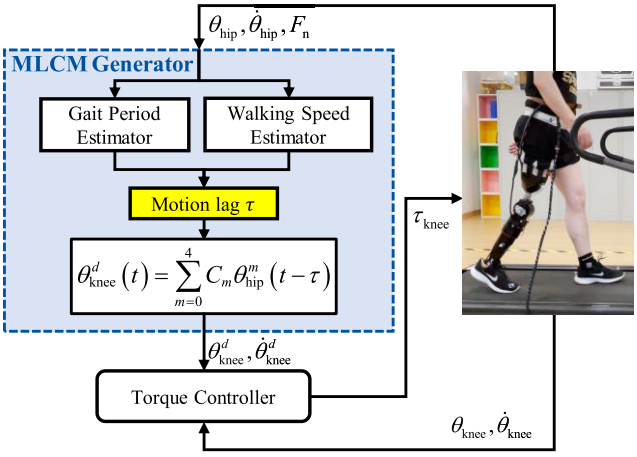

Fig. 3. Block diagram of the process of coordination control.

a PC through UART (universal asynchronous receiver and transmitter). The whole control loop operates at 100 Hz.

The sensing system consists of an IMU unit (MTi-630, Xsens, Netherland) for hip angle measurement, a 6-axis load sensor (M3713D, Sunrise Instruments, China) for ankle force measurement, and two incremental joint encoders (RLS, RM44D01, Slovenia) for knee and ankle joint motor angle measurement. The IMU provides signals of 3-axis acceleration, angular velocity, magnetometer, and Euler angles via a built-in algorithm. As the IMU is mounted on the anterior side of the thigh socket with the x-axis parallel to the ground, the x-axis Euler angle serves as the hip angle. An averaging filter is applied to the measured hip angle to eliminate the fluctuation caused by heel strikes. The load sensor's millivolt signal is amplified to volts through a signal amplifier and then passes through an ADC isolation module (AD7606, China) to mitigate electromagnetic interference. Subsequently, it communicates with the microprocessor via SPI. The signal is further processed through a decoupling matrix to obtain 3-axis force and moment components. The joint encoders, with an accuracy of $\pm 0.1°$, communicate with the actuator via a feedback cable, which transmits to the microprocessor via CAN.

III. Control Method

This section outlines the control strategy for the powered knee-ankle prosthesis, as illustrated in Fig.3. The control framework consists of an MLCM generator and a torque controller. Section III-A introduces the modified model based on MLCM established in previous research [17] and methods for gait period and speed estimation, which are used to calculate motion lag. We then discuss the hardware realization of motion lag and introduce the torque controller. In Section III-B, we conduct experiments to validate the accuracy of the speed estimation algorithm and to train the mapping model.

A. Control Loop

1) Modified MLCM (Motion-Lagged Coordination Mapping): In our gait model, the method of normalization has been revised from [17]. In the previous study, the input and output data are scaled to 0∼1 according to the maximum and minimum values of the current data. However, when it comes

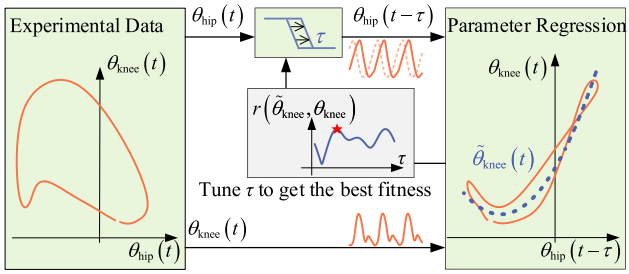

Fig. 4. Flowchart of the hip-knee MLCM construction.

to real-time control, the maximum and minimum values of the angle during the current gait cycle are not available. Thus, we determine a priori angle range based on the data of all experimental walking speeds. The hip angle minimum ($\theta_{hip,\,min}$) and maximum ($\theta_{hip,\,max}$) are set to -20 and 35°, and $\theta_{knee,\,min}$ and $\theta_{knee,\,max}$ to -5 and 65°, according to maximum and minimum values of the training dataset at various speeds. Then, the model coefficients are expressed as functions of the walking speed instead of constants in [17]. We also reduce the polynomial order from 4 to 2 because this lower order meets accuracy requirements while avoiding overfitting due to higher order terms. First, higher-order terms can amplify noise or jitter in the hip angle, leading to jitter in the knee angle. Second, higher-order terms can increase variations in gait among individuals, reducing the model's generalization performance. The modified model is given as follows:

$$\tilde{\theta}_{knee}(v,t) = \sum_{m=0}^{2} C_m(v)\left(\theta_{hip}(v,t-\tau)\right)^m,$$
$$C_m(v) = B_{0m} + B_{1m}v. \quad (1)$$

where v indicates the walking speed, $\theta_{hip}(v,t-\tau)$ is the scaled hip angle after translating the motion lag τ:

$$\theta_{hip}(v,t-\tau) = \frac{2\left(\theta_{hip,\,meas}(v,t-\tau) - \theta_{hip,\,min}\right)}{\left(\theta_{hip,\,max} - \theta_{hip,\,min}\right)} - 1, \quad (2)$$

where $\theta_{hip,\,meas}$ is the measured hip angle. $\tilde{\theta}_{knee}(v,t)$ denotes the scaled knee angle derived from the mapping, which has the following relationship with the desired knee angle $\theta_{knee,\,des}$:

$$\tilde{\theta}_{knee}(v,t) = \frac{2\left(\theta_{knee,\,des}(v,t) - \theta_{knee,\,min}\right)}{\left(\theta_{knee,\,max} - \theta_{knee,\,min}\right)} - 1. \quad (3)$$

By Eqs. (2) and (3), hip and knee angles are scaled to -1∼1 to eliminate the magnitude difference of hip and knee angle so that the mapping parameters can be less sensitive to differences in scale.

MLCM parameters consist of τ and $C_m(v)$. The determination of τ follows the process shown in Fig. 4. Initially, the hip angle is shifted backward by a candidate motion lag (spanning from 0 to one gait period). Subsequently, the knee angle is mapped using the least squares method with Eq. (1). The motion lag τ is determined by maximizing the correlation coefficient $r\left(\tilde{\theta}_{knee}, \theta_{knee}\right)$ between the experimental and mapped knee angles. To determine $C_m(v)$, we need to train uniformly on the data for all speeds. First, we concatenate the motion-lagged hip angles across all walking speeds to form

the input $\mathbf{x}$ and assemble the corresponding knee angles to form the output $\mathbf{y}$.

$$\mathbf{x} = \begin{pmatrix} 1 & \dots & 1 \\ v_1 & \dots & v_K \\ \theta_{\text{hip},v_1} & \dots & \theta_{\text{hip},v_K} \\ v_1\theta_{\text{hip},v_1} & \dots & v_K\theta_{\text{hip},v_K} \\ \theta^2_{\text{hip},v_1} & \dots & \theta^2_{\text{hip},v_K} \\ v_1\theta^2_{\text{hip},v_1} & \dots & v_K\theta^2_{\text{hip},v_K} \end{pmatrix}^T,$$

$$\theta_{\text{hip},v_i} = \begin{pmatrix} \theta_{\text{hip}}\left(v_i, t_N - \tau_{v_i} + \Delta t\right) \\ \dots \\ \theta_{\text{hip}}\left(v_i, t_N\right) \\ \theta_{\text{hip}}\left(v_i, t_1\right) \\ \dots \\ \theta_{\text{hip}}\left(v_i, t_N - \tau_{v_i}\right) \end{pmatrix}^T, \tag{4}$$

$$\mathbf{y} = \begin{pmatrix} \theta_{\text{knee},v_1} & \dots & \theta_{\text{knee},v_K} \end{pmatrix}^T,$$

$$\theta_{\text{knee},v_i} = \left(\theta_{\text{knee}}\left(v_i, t_1\right) \dots \theta_{\text{knee}}\left(v_i, t_N\right)\right). \tag{5}$$

The subscript i in v_i represents the i-th of K walking speeds. N denotes the total number of sampling points in a gait cycle, and Δt represents the time interval between two sampling points. The mapping parameters can be expressed as:

$$\mathbf{\Phi} = \begin{pmatrix} B_{00} & B_{10} & B_{01} & B_{11} & B_{02} & B_{12} \end{pmatrix}^T. \tag{6}$$

Using Eqs. (4)-(6), Eq. (1) can be expressed in matrix form:

$$\mathbf{y} = \mathbf{x}\Phi. \tag{7}$$

Finally, $\mathbf{\Phi}$ can be solved by:

$$\mathbf{\Phi} = \left(\mathbf{x}^T\mathbf{x}\right)^{-1}\mathbf{x}^T\mathbf{y}. \tag{8}$$

Fig. 4 illustrates the effectiveness of MLCM. Before shifting the hip motion, each hip angle can be mapped to two different knee angles. Conversely, after applying the motion lag, each hip angle aligns with two similar knee angles. This phenomenon explains the necessity of motion lag in the mapping process. Nevertheless, it is impractical to determine by iterating through all possible values in real-time control.

Interestingly, we found an alternative way to calculate τ. According to our statistical analysis [17], τ can be expressed as a function of walking speed v and gait period T as follows:

$$\tau = A_0 + A_1 vT + A_2 T. \tag{9}$$

Here A_0, A_1, and A_2 are obtained by fitting the experimental data. Thus, in real-time control, the motion lag can be determined once the walking speed and gait period are estimated. The algorithms for the gait period and walking speed estimation are detailed below.

2) Gait Period Estimation: The gait cycle is generally defined as the interval between two heel strike moments. Heel strike timing is commonly determined using a load sensor on the ankle, which detects pressure changes. A heel strike is considered to have occurred at the end of the swing phase when F_z (the axial pressure of the load sensor) was greater than a threshold value of F_{z0}(calibration value when the prosthesis is off the ground) +50 N. Then the gait period is calculated as follows:

$$T_{\text{est}}(n) = \text{Heelstrike}(n) - \text{Heelstrike}(n-1). \tag{10}$$

Here n denotes the n-th gait cycle. This method is suitable for a stable gait. To prevent incorrect estimation due to unstable gait when the participant starts and stops, we set the gait period threshold value in the range of 0.9∼2.0 s.

3) Walking Speed Estimation: Speed estimation methods can be divided into two categories: (1) machine learning algorithms and (2) analytical algorithms based on kinematic models. Machine learning algorithms have achieved a small RMSE of 0.070±0.007 m/s when estimating walking speed [19]. However, these data-driven algorithms require substantial training data, abundant sensor information, and a lot of model parameters, making online deployment challenging. In contrast, analytical algorithms can attain comparable estimation accuracy while avoiding these drawbacks. For example, [20] assumes the lower limb as an inverted pendulum model, estimating speed by considering the forward movement distance of the pendulum's endpoint as a half-step stride length. This method only needs one thigh-mounted IMU and finally realized an RMSE of 0.036±0.021 m/s. Because of its simplicity and accuracy, we use this approach in real-time control. In this method, the stride, defined as the moving distance of the center of mass (CoM) during one gait cycle, can be calculated as

$$x_{\text{stride}} = 2l_{\text{leg}}\left(\sin\left(\theta^h_{\max}\right) + \sin\left(\text{abs}\left(\theta^h_{\min}\right)\right)\right). \tag{11}$$

Here, l_{leg} is the leg length of the subject, $\theta^h_{\max}$ and $\theta^h_{\min}$ are the maximum and minimum hip angles in the previous gait cycle. They are limited to 20∼35 (deg) and −25∼−10 (deg), respectively. Dividing the stride by the estimated gait period gives us an estimated walking speed:

$$v_{\text{est}} = x_{\text{stride}}/T_{\text{est}}. \tag{12}$$

v_{est} is limited to 1.5∼4.5 km/h to ensure that if there is foot scuffing, the estimated speed will be limited to a manageable range.

4) Hardware Realization of Motion Lag: Motion lag can be calculated by substituting the estimated gait period and speed into Eq. (9). To implement the motion lag in real-time control, we follow the approach in [21]. First, a float array with a length of L is defined to store the time history of the hip angle, namely $\mathbf{D}$. At the initial control cycle, the hip signal is written into D_1. In subsequent control cycles, the data in $\text{D}_{1:L-1}$ is copied to $\text{D}_{2:L}$, and then the current hip angle is written into D_1. Supposing the control frequency is f_c and the data at D_L is output, the motion lag between the input and output is given by $\tau = (L-1)/f_c$. This motion lag can be altered by changing L.

5) Torque Controller: By substituting the measured motion-lagged hip angle into the MLCM, the reference knee trajectory can be obtained. Motion control based on the reference trajectory is realized by a torque controller, which is formulated as follows:

$$M_{\text{knee}} = K_p \cdot \left(\theta^d_{\text{knee}} - \theta_{\text{knee}}\right) + K_d \cdot \left(\dot{\theta}^d_{\text{knee}} - \dot{\theta}_{\text{knee}}\right),$$
$$\theta_{\text{knee}} = \theta^M_{\text{knee}}/i_{\text{knee}}, \dot{\theta}_{\text{knee}} = \dot{\theta}^M_{\text{knee}}/i_{\text{knee}} \tag{13}$$

where θ_{knee} and $\dot{\theta}_{\text{knee}}$ are the angle and angular velocity of knee prosthesis, θ^M_{knee} and $\dot{\theta}^M_{\text{knee}}$ are the joint motor angle

measured by the encoder, i_{knee} is the transmission ratio, θ^d_{knee} ($= \theta_{\text{knee, des}}$ from Eq.(3)) and $\dot{\theta}^d_{\text{knee}}$ are the reference angle and angular velocity obtained from MLCM. $\dot{\theta}^d_{\text{knee}}$ is derived as the difference between θ^d_{knee} of the previous and the next sampling point.

B. Model Training and Evaluation

To determine the parameters of Eq. (9) and validate the speed estimation algorithm, we conducted gait experiments with one healthy subject (Subject 1, 170 cm, 63 kg). The subject walked on a treadmill with speeds varying from 2.0 km/h to 4.5 km/h in 0.5 km/h increments, each lasting two minutes. In the first minute, a walking mode with a small stride length was used. In the subsequent minute, a walking mode with a large stride length was used. The subject was allowed to self-select his stride. The choice of two distinct walking modes was motivated by Eq. (9), which relates walking speed to stride length and stride frequency. Thus, we aim to investigate how stride length changes might impact speed estimation accuracy. A motion capture system (Vicon, Oxford, UK) was utilized to record the lower-limb kinematic data during the whole process. Notably, there is a difference between the treadmill's displayed speed and the actual running belt speed. After calibration, the corresponding values for displayed speed and actual speed were determined as follows: 1.5 km/h (1.37 km/h), 2.0 km/h (1.82 km/h), 2.5 km/h (2.27 km/h), 3.0 km/h (2.76 km/h), 3.5 km/h (3.19 km/h), 4.0 km/h (3.67 km/h), and 4.5 km/h (4.13 km/h).

The above gait data with different walking speeds and stride lengths, after averaging over at least 20 gait cycles, formed our training dataset (7 speeds $\times$ 2 stride lengths $=$ 14 groups). These data were then normalized to -1 $\sim$ 1 by Eqs. (2) and (3) in the manuscript. Then, motion lag was obtained for each group of data by the way illustrated in Fig. 4. Next, these 14 groups of data with known gait periods, walking speeds, and motion lags were stitched together via Eq. (4) and Eq. (5) to form our input matrix (x) and output vector (y). Finally, by applying Eq. (8), the mapping coefficients ($\mathbf{\Phi}$) can be obtained. Their values are

$$\mathbf{\Phi} = \begin{pmatrix} -0.7104 & 0.0124 & -0.8533 & 0.0595 & 1.7419 & -0.0622 \end{pmatrix}^T.$$

For speed estimation, l_{leg} in Eq. (11) is set to 0.88 m based on the subject's physical parameters. The speed estimation errors are shown in Fig. 5. This figure shows that as the speed increases, the estimation error first decreases and then increases. At a speed of 2.76 km/h, the error reaches a minimum of below 0.1 km/h, and at a speed of 4.13 km/h, it reaches a maximum of around -0.25 km/h. At low speeds, the estimation error of small strides is larger than that of large strides, while the opposite is true at high speeds. But overall, regardless of the stride length and walking speed, the estimation errors are within an acceptable range and consistent with those reported in [20].

Although the empirical formula for motion lag in [17] is a function of walking speed and gait period, the previous work did not distinguish between long and short gait periods (large and small strides) at the same walking speed and calculated the motion lag separately. Therefore, we refitted the empirical

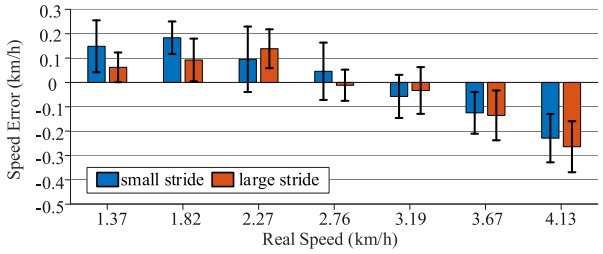

Fig. 5. Error of speed estimation.

formula for motion lag based on the data of Subject 1. The parameters in Eq. (9) are refitted as: $A_0 = 0.2681$, $A_1 = -0.0310$, $A_2 = 0.1077$. It is worth noting that if we unify the units and substitute vT in Eq. (9) to x_{stride}, the equation can be written as:

$$\tau = 0.2681 - 0.1116 \cdot x_{\text{stride}} + 0.1077 \cdot T. \tag{14}$$

We can see clearly the physical significance of motion lag from Eq.(14). Based on a baseline motion lag (A_0), the motion lag decreases with increasing stride length and increases with a longer gait period. In Section IV-A, we will further discover that the baseline motion lag is adjustable for different people.

IV. Experiments

This section describes the experimental protocol and results with speed adaptive walking of two non-disabled subjects and two transfemoral amputees wearing the powered knee prosthesis. An FSM-based impedance controller (FSMIC) is also proposed to benchmark the MLCM-based coordination controller (see Section S. II in Supplementary for details). This study was reviewed and approved by the Ethics Committee of Fudan University (No. FE23262I). The aims and details of the protocol were fully explained to the subjects with the signing of written informed consent.

A. Experiment Protocol

Two non-disabled subjects and two transfemoral amputees participated in this experiment, with the first non-disabled subject (Subject 1) being the same participant in Section III-B and the second non-disabled subject (Subject 2, 165 cm, 70 kg) serving for cross-validation. Each non-disabled subject was fit with the prosthesis using a leg bypass adapter (Fig. 6(a)). The physical parameters of two amputees (Subject 3 and 4) are shown in Table I. Three sets of experiments were conducted with each of the two control methods. The first set of experiments consisted of five round trips on a 3 m walkway without handrails. The amputees did not participate in the first set of experiments, because they were off the handrails while they were on the treadmill. The second set of experiments involved walking on a treadmill at several steady speeds for one minute each. Subject 1 completed walks at 1.82, 2.27, 2.76, 3.19, 3.67, and 4.13 km/h, while Subject 2 did not perform the 4.13 km/h walk as it was beyond his tolerance. Subject 3 completed walking at 2.0, 2.5, 3.0, and 3.5 km/h with the MLCMC and reached a maximum of 3.0km/h with the FSMIC. Subject 4 reached a maximum of 4.0 km/h with both controllers. The third set of experiments involved walking on a treadmill at variable speeds, increasing from 0 to the

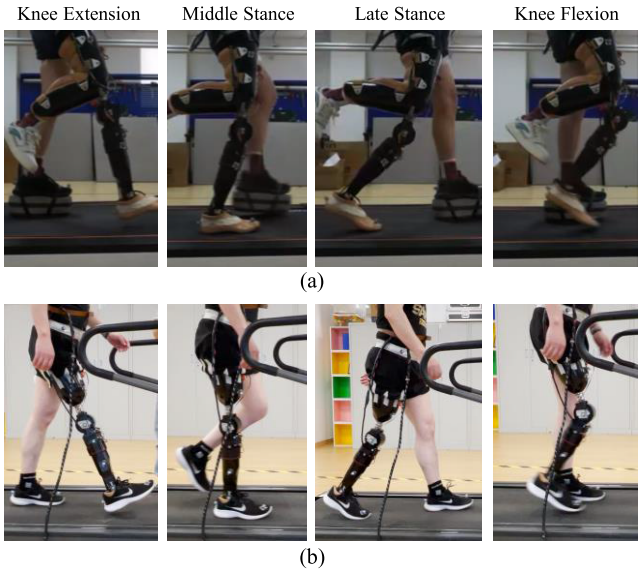

Fig. 6. Snapshots of (a) the non-disabled subject and (b) the amputee walking with the powered knee prosthesis. A shoe lift is added under the healthy foot to equalize leg lengths.

TABLE I
THE PHYSICAL PARAMETERS OF AMPUTEES

ID	Sex	Age	Height (cm)	Weight (kg)	Years wearing a prosthesis	Percentage of residual limb to healthy limb
3	Male	45	170	68	25	60%
4	Male	49	173	75	20	40%

customed maximum speed and then decreasing back to 0 km/h, with increments and decrements of 0.1 km/h per second. The non-disabled subjects both used handrails because it is hard to stay stable with a 10-cm-high shoe lift (Fig. 6(a)), while both amputees were off the handrails. A motion capture system (Vicon, Oxford, UK) was utilized to record the lower-limb kinematic data during the whole process. The STM32 sended the sensing information and estimates of the MLCMC to the computer at 100Hz through UART. It should be noted that before each experiment started, the subjects' prosthesis was held upright off the ground for 5 seconds to set the initial values of the IMU angle and the axial force to 0.

The knee controller for all subjects used the mapping model described in Section III-A, and mapping coefficients in Section III-B, with some individualized adjustments. The customizable parameters are the hip and knee maxima ($\theta_{\text{hip, min}}$, $\theta_{\text{hip, max}}$, $\theta_{\text{knee, min}}$, and $\theta_{\text{knee, max}}$ in Eqs.(2) and (3)), the baseline motion lag (A_0 in Eq.(9)), and the leg length (l_{leg} in Eq.(11)). Take Subject 3 as an example. The hip minimum was adjusted from -20° to -25° to accommodate his hip range of motion. A_0 was modified from 0.2681 to 0.25 to improve his comfort by reducing motion lag. The leg length was set to 0.805 m based on measurements. These adjustments demonstrated that while the mapping coefficients remain constant, refining the normalization range and baseline motion lag enhances the model's applicability to a broader range of amputees. Table II shows the values of customizable parameters for each subject. In addition to the measured l_{leg}, 7 parameters need to be individually adjusted for each subject. Except for K_{p} and K_{d}, All the parameters have a clear physical meaning and remain constants throughout the gait. Thus, they required less time to adjust compared to FSMIC. A detailed tuning process of K_p (unit: Nm/deg.) and K_d (unit: Nm/(deg./s)) is introduced in Section S.I of Supplementary.

TABLE II
CUSTOMIZABLE PARAMETERS FOR EACH SUBJECT

Name	Subject 1	Subject 2	Subject 3	Subject 4
K_{p} (Nm/deg.)	4.5, 1.6	4.5, 1.6	2.2	2.2
K_{d} (Nm/deg.)	0.3, 0.2	0.3, 0.2	0.25	0.25
$\theta_{\text{hip,max}}$(deg.)	35	35	35	35
$\theta_{\text{hip,min}}$(deg.)	-20	-20	-25	-25
$\theta_{\text{knee,max}}$(deg.)	65	65	65	70
$\theta_{\text{knee,min}}$ (deg.)	-5	-5	-5	-5
A_0 (s)	0.2681	0.2681	0.25	0.24
l_{leg} (m)	1.0	1.0	0.805	0.805

The ankle joint is controlled by a benchmark FSM-based impedance controller (see Section S.II in Supplementary for details) for non-disabled subjects and fixed to 0 degrees for transfemoral amputees. All amputee participants agreed that active control of the ankle joint is less important than knee joint control when walking on flat ground. They even felt that a passive elastic carbon-fiber foot would improve their walking comfort. Considering the practical needs of amputees, the active control of the ankle joint is disregarded currently.

B. Experiment Results

1) Walking Without Handrails: Both controllers can realize walking without handrails at a slow speed, as seen in the supplementary video. When walking on a treadmill, it is possible to walk without handrails at 1.82 or 2.27 km/h. Handrails are necessary at faster speeds for two reasons. One is because the healthy limb wears a shoe lift of about 12 cm, making the subject possibly fall or get injured at fast speeds. Another reason is attributed to the large weight of the prosthesis (about 4.5 kg in total), which leads to difficulties for the residual limb in lifting the prosthesis quickly without the help of handrails.

2) Steady-Speed Walking: MLCMC outperforms FSMIC in capturing lower limb kinematics changes with varying walking speeds. Fig. 7 shows that as speed increases, both non-disabled subject and intact limbs of amputee subject exhibit larger hip and knee swing amplitudes and enhanced flexion in response to heel strike impact. The FSMIC cannot adapt to the variation in the knee swing amplitude with walking speed due to its fixed 60° equilibrium position for the knee during the backward swing. Consequently, the hip joint must fully compensate for stride length variations caused by walking speed. As a result, the change of hip trajectory amplitude in FSMIC is much greater than that of non-disabled individuals, as shown in the hip RMSE in Fig.9. In contrast, MLCM closely mirrors the amplitude change in hip trajectory with walking speed observed in non-disabled individuals, thanks to the knee's increasing maximum angle and advanced swing phase with walking speed.

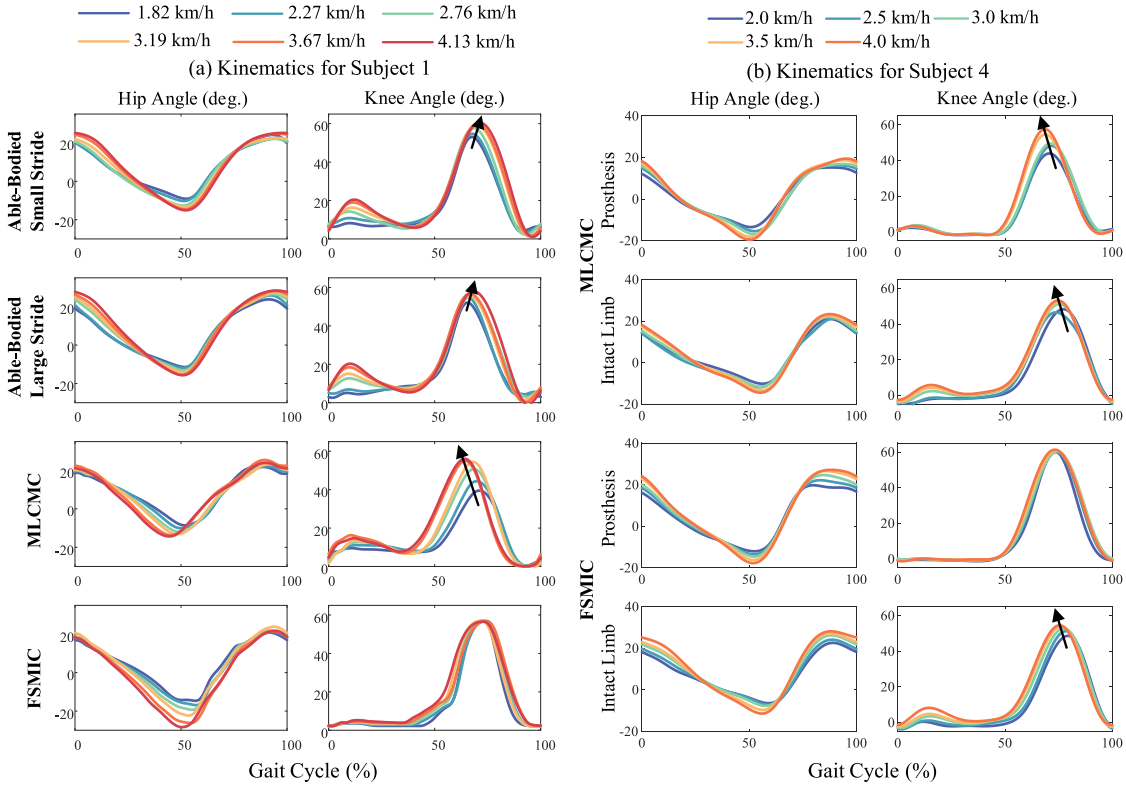

Fig. 7. The average kinematic trajectories generated by both controllers across varying treadmill speeds over 20 stabilized gait cycles for (a) Subject1 and (b) Subject4. Reference non-disabled trajectories for Subject 1 are obtained from the experiment in Section III-B. The gait cycle begins and ends with two heel strike moments. Roughly, the initial 60% of the gait cycle represents the stance phase, while the subsequent 40% corresponds to the swing phase. The black arrows represent the trend of the maximum knee angle as the walking speed increases.

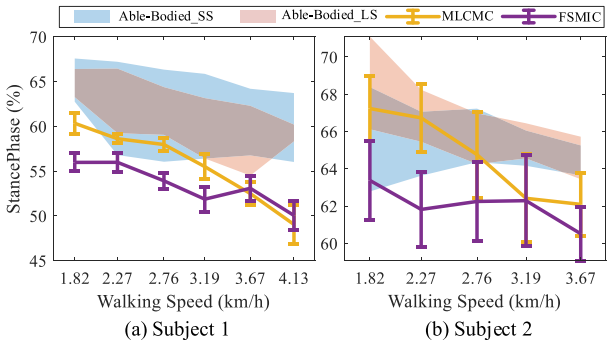

Fig. 8. Percentage of stance phase versus walking speed for (a) Subject 1 and (b) Subject 2. Error bars indicate ±1 standard deviation over at least 20 periods, with the shaded region representing the range enclosed by ±1 standard deviation. “non-disabled_SS” refers to non-disabled data without a prosthesis with a small stride, while “non-disabled_LS” represents that with a large stride. “MLCMC” and “FSMIC” denote actual stance phase percentages during prosthetic ambulation with different controllers.

MLCMC excels at capturing phase changes in variable speed motion compared to FSMIC. In Fig. 8, it is evident that as speed increases, both non-disabled subjects exhibit a decreased percentage of stance phase. While both controllers show this trend, MLCMC’s stance phase percentage closely aligns with that of healthy individuals, particularly at lower walking speeds. This suggests that MLCMC offers enhanced stability during the stance phase, promoting an increased duration of the stance phase by subjects. However, there is an issue of an early leg swing for MLCMC at 3.67 and 4.13 km/h in Subject 1’s results. This discrepancy may be attributed to the recalibration of the initial IMU angle in the experiments at these speeds.

We employed RMSE to quantify the similarity of the hip and knee trajectories obtained by the two controllers to those of non-disabled individuals or intact limbs (Fig. 9). MLCMC significantly reduces the compensatory behavior of hip joint, resulting in a smaller hip RMSE for all subjects. While MLCMC demonstrated a lower knee RMSE for almost all gaits of Subjects 1 and 2, it achieved exactly the opposite result on Subjects 3 and 4. One of the reasons for this may be that the motion lag of the MLCMC was not tuned to be optimal, resulting in a gap of several time points between the moment of emergence of the maximal value of the prosthetic knee and the healthy side. On the other hand, it is possible that the normalization factor of the mapping was not tuned to be optimal, resulting in the amplitude of the prosthetic knee being slightly smaller than that of the healthy limb. Nevertheless, considering the substantial reduction of hip RMSE compared to FSMIC, MLCMC has better overall gait consistency than FSMIC.

We also compared the stride length of both controllers (see Fig. 10). Among all the subjects, stride length increases with speed, a trend observed in both controllers. MLCMC’s variation in stride length closely resembles that of non-disabled individuals (Fig. 10(a) and (c)). MLCMC adjusts stride length for stability at different speeds, while FSMIC consistently exhibits longer strides due to excessive hip swing, leading to instability and risk of falls. Notably, the stride length difference for Subject 4 is small because his FSMIC parameters were adjusted to facilitate a smoother backward

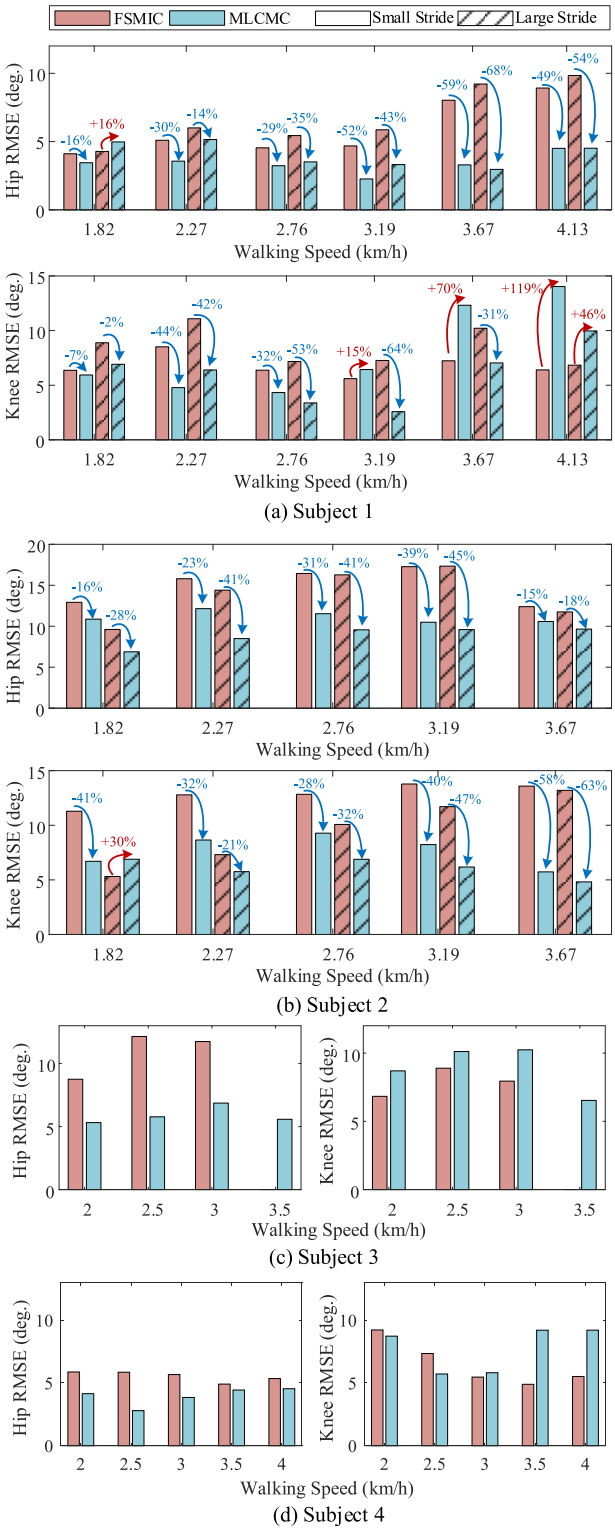

Fig. 9. The averaged RMSE of both controllers in observed kinematics relative to non-disabled walking data over 20 stabilized gait cycles for (a) Subject 1, (b) Subject 2, (c) Subject 3 and (d) Subject 4. Solid bars indicate the RMSE between observed kinematics and non-disabled kinematics with a small stride, while striped bars represent the RMSE between observed and non-disabled kinematics with a large stride.

swing (see Supplementary for details). Both controllers show similar stride variations between the intact and prosthetic limbs because the intact limb adjusts to maintain gait symmetry.

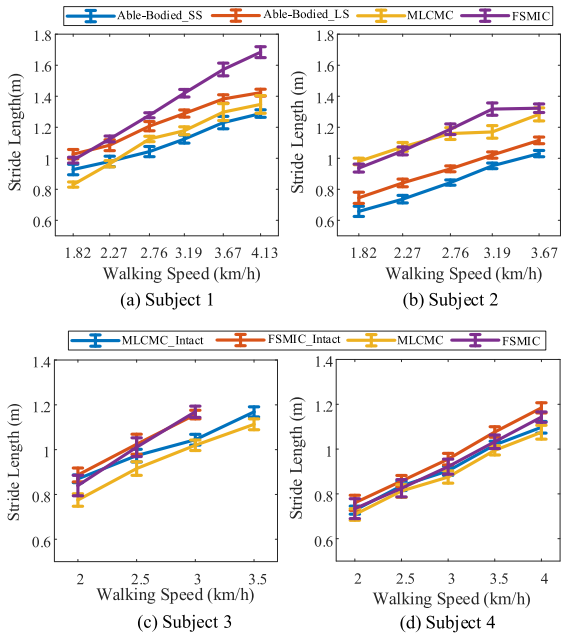

Fig. 10. Averaged stride length as a function of walking speed for (a) Subject1, (b) Subject2, (c) Subject3 and (d) Subject4. Error bars represent ±1 standard deviation over at least 20 periods. '_SS' represents the non-disabled data with a small stride, while '_LS' represents that with a large stride. '_Intact' represents the intact limb of the corresponding controller.

TABLE III
THE ABSOLUTE AVERAGE ERROR OF SPEED ESTIMATION

Actual Speed (km/h)	Estimated Error (km/h) Subject 1	Subject 2
1.82	0.59±0.07	0.31±0.04
2.27	0.37±0.12	0.21±0.09
2.76	0.19±0.08	0.29±0.12
3.19	0.19±0.10	0.37±0.15
3.67	0.03±0.16	0.09±0.13
4.13	0.11±0.20	\
Actual Speed (km/h)	**Estimated Error (km/h) Subject 3**	**Subject 4**
2	0.65±0.11	0.50±0.06
2.5	0.64±0.06	0.32±0.09
3.0	0.58±0.08	0.26±0.10
3.5	0.60±0.12	0.16±0.10
4.0	\	0.10±0.09

Table III presents the averaged speed estimation errors, which are crucial for motion lag determination. Subjects 1, 3, and 4 show a decreasing estimation error with increasing walking speed, while Subject 2's error fluctuates between 0.21 and 0.37 km/h, reaching a minimum of 0.09 km/h at 3.67 km/h. In addition, error fluctuations increase at higher walking speeds for both subjects due to reduced gait stability. Using Eq. (9), with a maximum error of 0.65 km/h and a maximum gait period of approximately 1.9 seconds (at 1.82 km/h), the calculated motion lag deviates by only 0.03 seconds from empirical values. The error diminishes with higher speeds because the gait period decreases as the speed increases. Although with motion lag bias, it is interesting that all subjects reported not feeling a significant lag in knee angle when walking. We speculate that motion lag robustness may benefit gait control, but now we cannot provide any more

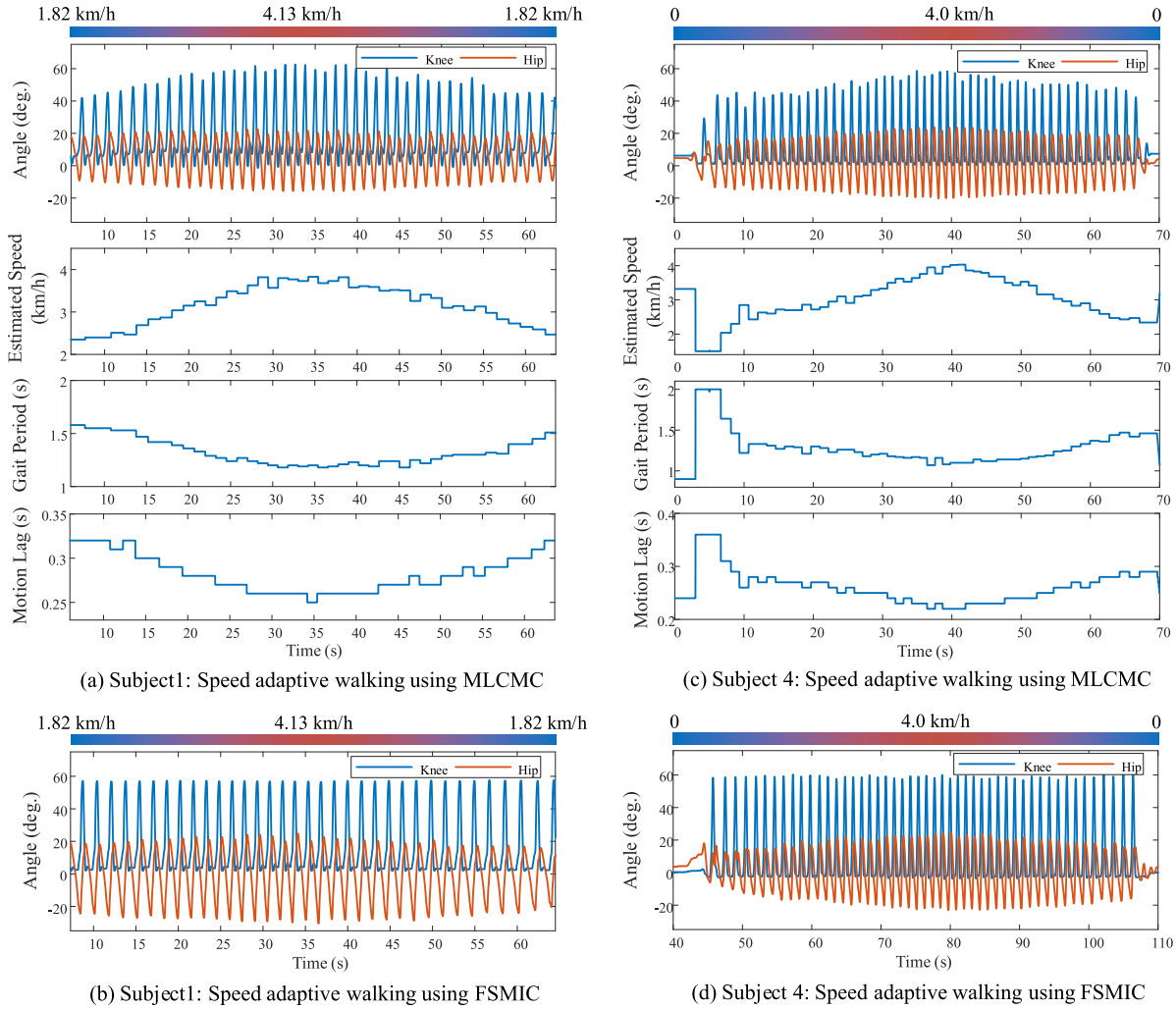

(a) Subject1: Speed adaptive walking using MLCMC

(c) Subject 4: Speed adaptive walking using MLCMC

(b) Subject1: Speed adaptive walking using FSMIC

(d) Subject 4: Speed adaptive walking using FSMIC

Fig. 11. Hip and knee trajectories produced by both controllers for speed adaptive walking task of Subject1 and Subject4. The estimated speed and motion lag by the MLCMC are also shown here to demonstrate the effectiveness of the estimation algorithm.

scientific evidence. A more in-depth theoretical analysis can be conducted in the future.

3) Speed Adaptive Walking: Continuous variable speed experiments highlight MLCMC's ability to autonomously adapt to speed changes. The kinematics results of both controllers for Subject 1 and Subject 4 are shown in Fig. 11 (see the Supplementary video for the whole walking process of all subjects). In MLCMC results, the amplitudes and frequencies of knee and hip motion increase synchronously with the walking speed, demonstrating good coordination. In Subject 1, the maximum knee flexion angle changes from 41.65° to 61.84°, while the minimum hip angle shifts from −9.2° to −15.69°. For Subject 4, the maximum knee flexion angle varies from 29.35° to 58.43°, and the minimum hip angle transforms from −8.80 to −20.26°. In contrast, FSMIC's fixed impedance parameters prevent the knee joint from adjusting amplitude, resulting in significant amplitude variations in the hip joint during variable speed walking. In Subjects 1 and Subject 4, the minimum hip angles at maximum walking speed reach −29.91° and −23.12°, respectively, demonstrating an increase of 35% and 14%, compared to the values obtained with MLCMC. This compensatory behavior requires more effort from the participants when changing speed. Additionally, in the final seconds of Subject 2's deceleration and the initial seconds of Subject 3's acceleration, a failure occurs during the knee's transition to the swing phase (see Supplementary video), indicating a misrecognition issue with FSMIC. The comparison between the two controllers demonstrates that inter-joint coordination in knee control can result in a more natural gait.

The trend of motion lag with walking speed is accurately estimated. Since the gait period, walking speed, and motion lag are updated once per cycle, these three parameters vary in a stepwise manner on the time scale. Fig. 11 demonstrate that the gait period varies continuously during acceleration and exhibits step-like shifts during deceleration. This suggests that the prosthesis increases the step frequency for acceleration and reduces the step length for deceleration. Thanks to motion lag estimation accounting for both the step frequency (the reciprocal of the gait period) and stride length (walking speed × gait period), the MLCMC controller is suitable for both walking modes and realizes smooth switching.

The results for Subject4 in Fig.11 included a standstill to demonstrate that the MLCMC also supports start-to-walk and sudden stops. Note that at the beginning and end of MLCMC walking, there are two instances of misestimating walking

speed, gait period, and motion lag. When the subjects did not start walking or suddenly stop, the estimated speed was approximately 3.3 km/h. This is because $\theta^h_{\max}$ and $\theta^h_{\min}$ in Eq. (11) and gait period were all set to the limit values (20° for $\theta^h_{\max}$, -10° for $\theta^h_{\min}$, and 0.9 s for the gait period, according to Section III-A.3 and III-A.4) since they cannot be updated correctly while standing still. Although this resulted in an inaccurate estimation of the motion lag, the mapped knee angle remained essentially constant since the hip angle did not change significantly after stopping. Consequently, the prosthesis can be maintained in an upright position immediately after a sudden stop. The same applied to the transition from standing to walking. When starting to walk slowly from a standing position, the knee joint can keep up with the hip joint movement. However, it cannot keep up if the speed changes too rapidly.

V. Discussion

A. Advantages of the Coordination Control Method

This study presented a hip-knee-coordination-based controller for the powered knee prosthesis that can autonomously adapt its performance across a wide range of walking speeds, verifying the feasibility of the MLCM proposed in [17]. The experiments involved four subjects, with the mapping trained using Subject 1's data and successfully applied to all subjects. All subjects reported that MLCMC enhances walking smoothness and efficiency. For Subject 1, MLCMC outperformed FSMIC in aspects of hip kinematic error, stance phase percentage, and stride length. Subjects 2, 3, and 4, which were cross-validated, also experienced better results with MLCMC in these aspects. As a result, all subjects found walking with MLCMC easier than with FSMIC. In the future, we will apply this method to more amputees to affirm the possibility of generalizing our mapping to a broader population, as stated in [17].

MLCMC significantly reduces control parameters compared to traditional FSMIC, thereby greatly reducing configuration time for prosthesis users. FSMIC has 17 control parameters for the knee joint, whereas MLCMC has only 7. The adjustment of impedance parameters in FSMIC, influenced by various gait phase classification criteria and equilibrium position choices, consumes an entire day, according to our actual experience. Nevertheless, FSMIC does not achieve optimal walking performance, such as the slight knee flexion in the early stance phase, which remains insignificant. In addition, some misrecognition of gait phases occurred in the experiments with FSMIC (see the supplementary video for some misrecognition moments). In contrast, MLCMC only needs to adjust appropriate K_{p} and K_{d}, hip and knee normalization factors, and baseline motion lag. With roughly 10 minutes of calibration, subjects can achieve a continuous, synergistic variable-speed walking experience.

Hip-angle-based MLCMC offers the potential for volitional prosthesis control. In our first set of experiments walking across a 3 m walkway, the subjects occasionally needed to take one or two steps in place for turning. When using MLCMC, the knee flexion remained minimal, mirroring the hip angle's slight movement, similar to a healthy person's maneuvering in place. In contrast, FSMIC causes unexpected knee swings when the prosthesis leaves the ground because of the finite state machine setting. MLCMC also holds promise for voluntary tasks such as obstacle crossing. According to [25], hip angle extension will increase when encountering obstacles. An increased hip extension of 40° will correspond to a 74° knee angle with MLCMC, which is enough to cross a 15 cm-high obstacle, according to [25]. Experiments in this regard can be explored in future research.

MLCMC can adapt walking speed by changing stride length or stride frequency, and it is comfortable switching between the two modes, which is closer to how a healthy person walks. Since motion lag is a function of both gait speed and period, different gait periods (different stride lengths) at the same speed will result in different motion lags. Thus, the knee trajectory can be adjusted according to the gait period (stride length) even at the same walking speed. Therefore, we believe that the MLCMC can be adapted to the changing speed habits of different people, whether they choose a small stride length to increase walking stability or a large stride length to minimize residual limb impingement. In contrast, the FSMIC only has the option of increasing stride length when walking speed increases (Fig.10(a)), possibly because the performance of the motor cannot support a faster cadence.

The introduction of motion lag in the control reduces the need for real-time prosthesis performance. It ensures that data delays due to filtering or communication do not affect the control. For example, the delay in the hip angle due to average filtering does not affect the control's real-time performance because it can be subtracted from the calculated motion lag since it is definitely smaller than the motion lag.

B. Limitations of the Study

The ankle controller in this study still uses FSMIC because we have not yet established a hip-ankle or knee-ankle mapping. On the other hand, for the sake of controlling variables, the ankle controller has to be kept in line with FSMIC. Meanwhile, amputees reported that active control of the ankle is less important than that of the knee. Instead, they preferred the ankle to be a passive elastic carbon-fiber foot. However, for studying lower limb synergy, it makes sense to establish a coordination mapping for the ankle. Unfortunately, translating the motion lag and establishing a coordination mapping does not work for the ankle joint, which means more inputs may be needed to predict the ankle motion. For example, [23] employs data from multiple past time points of the ankle and knee (or hip) as inputs to a NARX (nonlinear autoregressive model with exogenous inputs [24]) model to predict current ankle motion. According to [23], using data from 19 time points can yield an RMSE of less than 5°. Future work can explore convex optimization, sparse regression, or alternative approaches to reduce model inputs and use them for ankle prosthesis control.

Due to the limitations of the experimental conditions, heel strike moments in healthy individuals were determined using the lowest point of the heel marker's vertical motion, potentially introducing a slight error in heel strike timing. In contrast, the prosthesis's heel strike moment is accurately

measured via the force sensor on the ankle. The data discrepancy in healthy individuals may explain why Subject 1 did not exhibit the typical pattern of advancing the swing phase with increasing walking speed. While this limitation may influence the kinematic error calculations, it does not impact the rest of the analysis.

The accuracy of the walking speed estimation algorithm still needs to be improved. Incorrect step speed estimation can lead to incorrect motion lag. Although the calculated error of motion lag caused by speed estimation inaccuracies is slight, as discussed in Table I, improving the accuracy of walking speed estimation is still necessary for more accurate control. Approaches to achieve this may involve constructing a more comprehensive lower limb kinematics multilink model [16] or adding an extra IMU sensor to the foot to estimate the walking speed directly from the foot displacement [22].

This study has a limited number of subjects. While we anticipate MLCM's broader applicability, some adjustments are necessary. For example, hip and knee angle ranges for normalization may vary among individuals. Fine-tuning of motion lag is also required based on individual usage experience. However, the polynomial order and coefficients of MLCM remain unchanged.

VI. Conclusion

This study introduced a modified hip-knee-coordination-based controller for powered knee prostheses, showcasing its autonomous adaptability across a wide range of walking speeds, thereby confirming the feasibility of MLCM. An effective real-time motion-lag estimation algorithm was proposed to adapt to the variation in walking speed. Two non-disabled subjects and two transfemoral amputees wearing prostheses demonstrated MLCMC's superiority over FSMIC in terms of hip kinematic error, stance phase percentage, and stride length. Compared to FSMIC, MLCMC significantly reduces control parameters from 17 to 7, and avoids misrecognition during gait phase transitions, providing a straightforward, continuous, and coordinative control approach for prosthetic limbs.

Acknowledgment

The authors would like to thank Chang Lu, Chao Chen, Chaoyu Song, and Pengyu Zhou for their support and advice during the experiments and also would like to thank the Editor-in-Chief, the associate editors, and the anonymous reviewers for their constructive comments, based on which the presentation of this article will be significantly improved.

References

[1] T. Elery, S. Rezazadeh, E. Reznick, L. Gray, and R. D. Gregg, "Effects of a powered knee-ankle prosthesis on amputee hip compensations: A case series," *IEEE Trans. Neural Syst. Rehabil. Eng.*, vol. 28, no. 12, pp. 2944–2954, Dec. 2020.

[2] E. L. Bukowski, "Atlas of amputations and limb deficiencies: Surgical, prosthetic, and rehabilitation principles, ed 3," *Phys. Therapy*, vol. 86, no. 4, pp. 595–596, Apr. 2006.

[3] M. R. Tucker et al., "Control strategies for active lower extremity prosthetics and orthotics: A review," *J. Neuroeng. Rehabil.*, vol. 12, no. 1, pp. 1–30, 2015.

[4] F. Sup, A. Bohara, and M. Goldfarb, "Design and control of a powered transfemoral prosthesis," *Int. J. Robot. Res.*, vol. 27, no. 2, pp. 263–273, Feb. 2008.

[5] S. Gao, J. Mai, J. Zhu, and Q. Wang, "Mechanism and controller design of a transfemoral prosthesis with electrohydraulic knee and motor-driven ankle," *IEEE/ASME Trans. Mechatronics*, vol. 26, no. 5, pp. 2429–2439, Oct. 2021.

[6] A. F. Azocar, L. M. Mooney, J.-F. Duval, A. M. Simon, L. J. Hargrove, and E. J. Rouse, "Design and clinical implementation of an open-source bionic leg," *Nature Biomed. Eng.*, vol. 4, no. 10, pp. 941–953, Oct. 2020.

[7] Y. Wen, M. Li, J. Si, and H. Huang, "Wearer-prosthesis interaction for symmetrical gait: A study enabled by reinforcement learning prosthesis control," *IEEE Trans. Neural Syst. Rehabil. Eng.*, vol. 28, no. 4, pp. 904–913, Apr. 2020.

[8] E. J. Rouse, L. J. Hargrove, E. J. Perreault, and T. A. Kuiken, "Estimation of human ankle impedance during the stance phase of walking," *IEEE Trans. Neural Syst. Rehabil. Eng.*, vol. 22, no. 4, pp. 870–878, Jul. 2014.

[9] T. Lenzi, L. Hargrove, and J. Sensinger, "Speed-adaptation mechanism: Robotic prostheses can actively regulate joint torque," *IEEE Robot. Autom. Mag.*, vol. 21, no. 4, pp. 94–107, Dec. 2014.

[10] N. Thatte, T. Shah, and H. Geyer, "Robust and adaptive lower limb prosthesis stance control via extended Kalman filter-based gait phase estimation," *IEEE Robot. Autom. Lett.*, vol. 4, no. 4, pp. 3129–3136, Oct. 2019.

[11] D. J. Villarreal and R. D. Gregg, "Unified phase variables of relative degree two for human locomotion," in *Proc. 38th Annu. Int. Conf. IEEE Eng. Med. Biol. Soc. (EMBC)*, Aug. 2016, pp. 6262–6267.

[12] D. J. Villarreal, H. A. Poonawala, and R. D. Gregg, "A robust parameterization of human gait patterns across phase-shifting perturbations," *IEEE Trans. Neural Syst. Rehabil. Eng.*, vol. 25, no. 3, pp. 265–278, Mar. 2017.

[13] D. Quintero, D. J. Villarreal, D. J. Lambert, S. Kapp, and R. D. Gregg, "Continuous-phase control of a powered knee–ankle prosthesis: Amputee experiments across speeds and inclines," *IEEE Trans. Robot.*, vol. 34, no. 3, pp. 686–701, Jun. 2018.

[14] R. J. Cortino, T. Kevin Best, and R. D. Gregg, "Data-driven phase-based control of a powered knee-ankle prosthesis for variable-incline stair ascent and descent," *IEEE Trans. Med. Robot. Bionics*, vol. 6, no. 1, pp. 175–188, Feb. 2024.

[15] S. Rezazadeh, D. Quintero, N. Divekar, E. Reznick, L. Gray, and R. D. Gregg, "A phase variable approach for improved rhythmic and non-rhythmic control of a powered knee-ankle prosthesis," *IEEE Access*, vol. 7, pp. 109840–109855, 2019.

[16] T. K. Best, C. G. Welker, E. J. Rouse, and R. D. Gregg, "Data-driven variable impedance control of a powered knee–ankle prosthesis for adaptive speed and incline walking," *IEEE Trans. Robot.*, vol. 39, no. 3, pp. 2151–2169, Jun. 2023.

[17] Y. Lv, J. Xu, H. Fang, X. Zhang, and Q. Wang, "Data-mined continuous hip-knee coordination mapping with motion lag for lower-limb prosthesis control," *IEEE Trans. Neural Syst. Rehabil. Eng.*, vol. 30, pp. 1557–1566, 2022.

[18] T. Elery, S. Rezazadeh, C. Nesler, and R. D. Gregg, "Design and validation of a powered knee–ankle prosthesis with high-torque, low-impedance actuators," *IEEE Trans. Robot.*, vol. 36, no. 6, pp. 1649–1668, Dec. 2020.

[19] K. Bhakta, J. Camargo, W. Compton, K. Herrin, and A. Young, "Evaluation of continuous walking speed determination algorithms and embedded sensors for a powered knee & ankle prosthesis," *IEEE Robot. Autom. Lett.*, vol. 6, no. 3, pp. 4820–4826, Jul. 2021.

[20] Y. Liu, H. An, H. Ma, and Q. Wei, "Online walking speed estimation based on gait phase and kinematic model for intelligent lower-limb prosthesis," *Appl. Sci.*, vol. 13, no. 3, p. 1893, Feb. 2023.

[21] X. Zhang, J. Xu, and J. Ji, "Modelling and tuning for a time-delayed vibration absorber with friction," *J. Sound Vib.*, vol. 424, pp. 137–157, Jun. 2018.

[22] R. L. Medrano, G. C. Thomas, C. G. Keais, E. J. Rouse, and R. D. Gregg, "Real-time gait phase and task estimation for controlling a powered ankle exoskeleton on extremely uneven terrain," *IEEE Trans. Robot.*, vol. 39, no. 3, pp. 2170–2182, Jun. 2023.

[23] M. Eslamy and A. F. Schilling, "Estimation of knee and ankle angles during walking using thigh and shank angles," *Bioinspiration Biomimetics*, vol. 16, no. 6, Nov. 2021, Art. no. 066012.

[24] M. Münchhof and R. Isermann, *Identification of Dynamic Systems: An Introduction With Applications*, vol. 85. Heidelberg, Germany: Springer, 2011.

[25] J. Mendez, S. Hood, A. Gunnel, and T. Lenzi, "Powered knee and ankle prosthesis with indirect volitional swing control enables level-ground walking and crossing over obstacles," *Sci. Robot.*, vol. 5, no. 44, Jul. 2020, Art. no. eaba6635.